Since January 2020 Elsevier has created a COVID-19 resource centre with free information in English and Mandarin on the novel coronavirus COVID-19. The COVID-19 resource centre is hosted on Elsevier Connect, the company's public news and information website.

Journal of Hazardous Materials 301 (2016) 547–553

Contents lists available at ScienceDirect

Journal of Hazardous Materials

journal homepage: www.elsevier.com/locate/jhazmat

Evaluation of Ag nanoparticle coated air filter against aerosolized virus: Anti-viral efficiency with dust loading

Yun Haeng Joe, Dae Hoon Park, Jungho Hwang*

School of Mechanical Engineering, Yonsei University, Seoul 120-749, Republic of Korea

HIGHLIGHTS

- Ag particles were synthesized via spark discharge system and coated on the air filter.
- An anti-viral ability of the filter was evaluated against aerosolized virus particles with dust loading.
- A mathematical model of an anti-viral efficiency with dust loading was carried out.

GRAPHICAL ABSTRACT

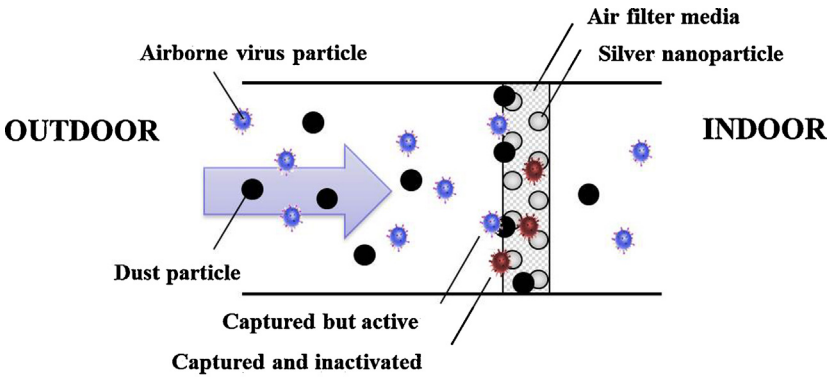

Anti-viral action with dust loading

ARTICLE INFO

Article history:
Received 23 June 2015
Received in revised form 18 August 2015
Accepted 8 September 2015
Available online 11 September 2015

Keywords:
Airborne virus
Dust loading
Inactivation
Silver nanoparticles

ABSTRACT

In this study, the effect of dust loading on the anti-viral ability of an anti-viral air filter was investigated. Silver nanoparticles approximately 11 nm in diameter were synthesized via a spark discharge generation system and were used as anti-viral agents coated onto a medium air filter. The pressure drop, filtration efficiency, and anti-viral ability of the filter against aerosolized bacteriophage MS2 virus particles were tested with dust loading. The filtration efficiency and pressure drop increased with dust loading, while the anti-viral ability decreased. Theoretical analysis of anti-viral ability with dust loading was carried out using a mathematical model based on that presented by Joe et al. (J. Hazard. Mater.; 280: 356-363, 2014). Our model can be used to compare anti-viral abilities of various anti-viral agents, determine appropriate coating areal density of anti-viral agent on a filter, and predict the life cycle of an anti-viral filter.

1. Introduction

The social requirements for removing and inactivating bioaerosols have increased due to increasing human indoor activities and rapid urbanization [1]. In particular, recent global illnesses caused by viral respiratory infections, such as severe acute respiratory syndrome (SARS) coronavirus and novel swine-origin

* Corresponding author Fax: +82 2 312 2821.
E-mail addresses: kazamajo@nate.com (Y.H. Joe), dhoonpark@yonsei.ac.kr (D.H. Park), jh@yonsei.ac.kr (J. Hwang).

http://dx.doi.org/10.1016/j.jhazmat.2015.09.017
0304-3894/

influenza A (H1N1), have led to concern regarding airborne viral infections [2,3]. Since virus particles, which are infectious and toxigenic [4–8], are only nanometers in size, they can remain suspended in the air long enough to be dispersed [9]. Since airborne infection is caused by these infectious aerosol particles, and the average person spends most of his/her time indoors [10], development of efficient air control technology is important for maintaining a clean indoor air environment and for preventing infection and spread of respiratory infectious diseases.

Recently, technologies including electrostatic precipitator (ESP), mechanical heating system, and antimicrobial agent (such as tea tree, eucalyptus oil, and carbon nanotube (CNT))-coated air filter have been tested for controlling and inactivating airborne virus particles [11–14]. In our previous study, aerosolized bacteriophage MS2 virus was inactivated with synthesized SiO_2-Ag nanoparticles, which were 400 nm silica particles decorated with 30 nm silver nanoparticles [15]. These particles were coated onto filter media using a conventional flow process, and the anti-viral ability of the fabricated filter was tested in the continuous airflow condition. However, in that study, all of the experiments were performed in clean air without consideration of dust particles. According to a report from the American Society of Heating, Refrigerating, and Air-conditioning Engineers (ASHRAE), dust particles can affect the growth of microorganisms captured on an antimicrobial-treated air filter [16]. Moreover, dust particles captured on the filter media can decrease the anti-microbial ability of a silver nanoparticle-coated air filter and increase the pressure drop across filter media [17].

Research on silver nanoparticles as antiviral agents is common. Even though the exact action mechanism of silver on virus particles is still unknown, remarkable results have been published. The high binding affinity of silver nanoparticles for hepatitis B virus (HBV) DNA and extracellular virion can inhibit the production of RNA and extracellular virion [18]. Silver ions (Ag^+) and silver nanoparticles react with sulfhydra, amino, carboxyl, phosphate, and imidazole groups of virus particles and denature the enzymes [19–23].

Various methods used to synthesize silver nanoparticles include spark discharge generation (SDG), which is a well-known simple and eco-friendly process [24–27]. The method is one of the mechanical methods using electrical discharge. When a high voltage is applied to a pair of close-set silver electrodes, a spark is produced between the two electrodes. The ions and electrons, which are accelerated by the electric field, impact the surface of the silver node and lead to vaporize electrode surface. The metallic vapors cool downstream from the spark. Finally, the silver nanoparticles are generated through nucleation, condensation, and coagulation processes [28,29].

In this study, silver nanoparticles were synthesized via the SDG system, and the particles were coated onto the air filter surface to provide anti-viral ability. The filtration ability of aerosolized MS2 virus particles and pressure drop across the filter with dust loading were evaluated. Then, anti-viral ability with dust loading was evaluated both experimentally and mathematically using a mathematical model, which was upgraded from the model presented in our previous work [15].

2. Materials and methods

2.1. Modeling

In our previous study [15], a mathematical model that predicts the temporal anti-viral ability of an anti-viral air filter was suggested as follows:

$$\eta_{\text{antiviral}}(t) = 1 - \exp\left[-\kappa \frac{\rho_{\text{agent}}}{\dot{N}''_{\text{depo}}}\text{t}\right] \quad (1)$$

$$\dot{N}''_{\text{depo}} = \eta_{\text{filt}}\dot{N}''_{\text{in}} \quad (2)$$

where ρ_{agent} is the coating areal density of the anti-viral agent (Ag nanoparticle in this study) on the filter surface (particles/cm^2), and t is the time. κ is a dimensionless value that represents the susceptibility of the virus against the anti-viral agent and depends on the types of virus and anti-viral agents and environmental conditions such as temperature and humidity. $\dot{N}''_{\text{depo}}$ is the virus deposition flux onto the filter (PFU/cm^2/min, PFU: plaque forming unit), which is determined using the filtration efficiency, η_{filt}, and the flux of upstream virus particles (PFU/cm^2/min), $\dot{N}''_{\text{in}}$. The number of surviving virus particles per unit area ($\dot{N}''_{\text{surv}}$, PFU/cm^2) can be calculated as follows;

$$N''_{\text{surv}} = \int_0^{\tau}(1-\eta_{\text{antiviral}}(t))\dot{N}''_{\text{depo}}dt = \dot{N}''_{\text{depo}}\tau\exp\left[-\kappa\frac{\rho_{\text{agent}}}{\dot{N}''_{\text{depo}}\tau}\right] + \kappa\rho_{\text{agent}}\text{Ei}\left[-\kappa\frac{\rho_{\text{agent}}}{\dot{N}''_{\text{depo}}\tau}\right] \quad (3)$$

where τ is the time during which virus particles are deposited onto the filter (15 mins in this study), and the function Ei(z) is the exponential integral function defined as

$$\text{Ei}(z) = -\int_{-z}^{\infty}\frac{e^{-t}}{t}\text{dt} \quad (4)$$

Then the fraction of surviving virus particles during the time interval of τ ($\phi_{\text{surv},\tau}$) is defined as follows:

$$\phi_{\text{surv},\tau} = \frac{N''_{\text{surv}}}{\dot{N}''_{\text{depo}}\tau} = exp\left[-\kappa\frac{\rho_{\text{agent}}}{\dot{N}''_{\text{depo}}\tau}\right] + \kappa\frac{\rho_{\text{agent}}}{\dot{N}''_{\text{depo}}\tau}\text{Ei}\left[-\kappa\frac{\rho_{\text{agent}}}{\dot{N}''_{\text{depo}}\tau}\right] \quad (5)$$

Assuming κ decreases with an increase in dust particles on the filter surface, κ can be modeled as follows:

$$\kappa = \frac{\kappa_0}{1+\gamma\rho_{\text{dust}}} \quad (6)$$

where ρ_{dust} is the areal density of dust particles on the filter surface (μg/cm^2), and γ (cm^2/μg) is a constant. The dimensionless parameter κ_0 refers to the susceptibility of virus particle to the anti-viral agent in the clean air condition (without dust).

2.2. Fabrication of the silver nanoparticle-coated air filter

In order to synthesize silver nanoparticles, a lab-made SDG system was used. The SDG system, which consisted of two silver electrodes (Ag-402651, Nilaco Corp., Japan), a power supply (UltraVolt, USA), and a simple RC circuit, was installed in front of the test duct (cross-section area: 4×4 cm^2 length: 100 cm) (Fig. 1a). A carrier gas of compressed clean air was passed through a clean air supply system at 5 LPM. The particles generated from the SDG system were delivered to the test duct by the carrier gas and were coated onto the filter under a continuous air flow condition. In this study, the supply voltage and current were set to 2 kV and 5 mA, respectively. The particle concentration upstream (C_{up}) and downstream (C_{down}) of the filter sample were measured using a scanning mobility particle sizer (SMPS, TSI Inc., USA) that consisted of a classifier controller (3080, TSI Inc., USA), a differential mobility analyzer (DMA, 3085, TSI Inc., USA), a condensation particle counter (CPC, 3775, TSI Inc., USA), and an aerosol charge neutralizer (Soft X-ray charger 4530, HCT Co., Ltd., Republic of Korea). The coating areal density (ρ_{agent}) of silver nanoparticles on the filter surface

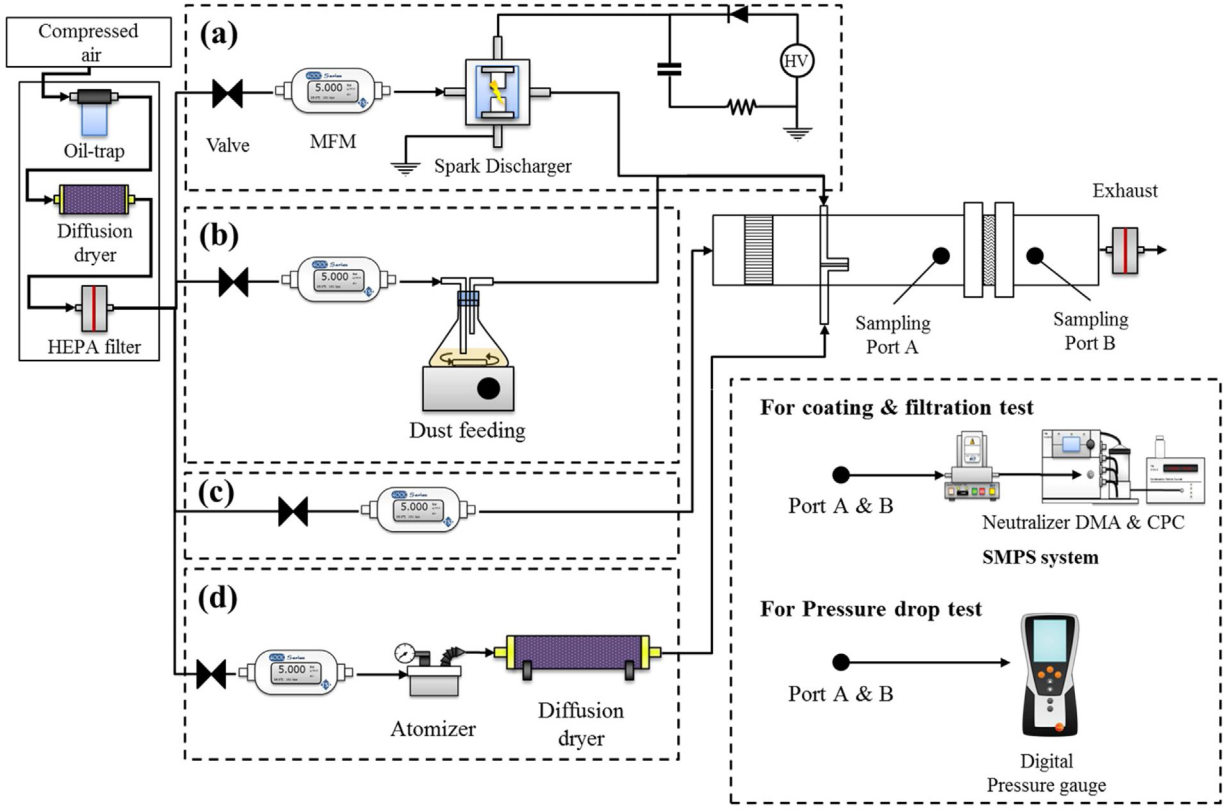

Fig. 1. Experimental setup for (a) anti-viral filter fabrication, (b) dust particle deposition, (c) pressure drop test and sheath air flow, and (d) filtration efficiency test.

was controlled by coating time and was calculated according to the following equation:

$$\rho_{agent} = \frac{Q\Delta t_c \left(C_{up} - C_{down}\right)}{A} \quad (7)$$

where Q is the flow rate, Δt_c is the coating time, and A is the area of the filter.

2.3. Dust loading on the filter media

In this study, Arizona road dust was used for dust loading. Arizona road dust is the compound used in the standardized air cleaner test (ISO 1203-1) and the Society of Automotive Engineers (SAE) test. Arizona road dust consists of 68–76% SiO_2, 10–15% Al_2O_3, and 2% to 5% Fe_2O_3. This composition is very similar to that of the atmosphere [30,31]. The test dust particles were aerosolized by a lab-made dust feeder that consisted of an Erlenmeyer flask and a magnetic stirrer and were flowed into the test duct at a volumetric flow rate of 5 LPM (Fig. 1b). The weight of the filter sample before and after dust loading was measured by an electronic precision balance (AR2140, OHAUS Corp., USA) in order to determine the loaded amount of dust. The pressure drop across the air filter sample at 5 LPM of air flow rate (velocity with no dust loading = 0.05 m/s) was measured by a digital pressure measuring device (Model 435-1, Testo, Germany), as shown in Fig. 1c, and the measured pressure drop was compared with the theoretical prediction carried out using the following equation [32]:

$$\Delta P = \frac{4\mu\alpha L u_0 (1 + 1.996Kn)}{0.25 d_f^2 \left\{-0.5\ln\alpha - 0.75 + \alpha - \frac{\alpha^2}{4} + 1.996Kn\left(-0.5\ln\alpha - 0.25 + \frac{\alpha^2}{4}\right)\right\}} \quad (8)$$

where L is the depth of the filter, μ is the dynamic viscosity of air, d_f is the diameter of the filter fiber, Kn is the Knudsen number, and u_0 is the media velocity, which can be defined as $Q/A(1-\alpha)$. The filter solidity, α, can be modeled according to the following equation:

$$\alpha = \alpha' + \alpha_{dust} \quad (9)$$

where α' is the solidity of a clean filter (without dust loading), and α_{dust} refers to the solidity added by the dust loading, which is defined by the following equation:

$$\alpha_{dust} = \frac{\text{volume of loaded dust}}{\text{volume of the sample}} = \frac{\rho_{dust} A/\rho_p}{AL} \quad (10)$$

In this study, effective dust particle density, ρ_p, was set as 3.1 g/cm^3 based on the chemical composition of Arizona road dust. Generally, a used filter is replaced when the pressure drop across the filter doubles that of the initial state. Thus, four cases of dust loading, 0 (without dust), 645 ± 86, 920 ± 98, and 1478 ± 128 μg/cm^2 were selected (the pressure drop increased by approximately two times higher when ρ_{dust} = 1478 ± 128 μg/cm^2). Medium grade glass fiber filters with a 0.04 ± 0.005 cm thickness, 0.0095 ± 0.0003 solidity, and 1.08 ± 0.36 μm fiber diameter, were chosen as the test filter media.

2.4. Preparation of virus solution

The aerosolized bacteriophage MS2 virus (ATCC 15597-B1) was used as the test virus. In order to prepare the virus solution, 0.1 mL of virus stock (initial titer: 10^{11} PFU/mL) was defrosted at room temperature and poured into 50 mL of de-ionized water (DI water).

2.5. Filtration of aerosolized bacteriophage MS2

The virus solution was aerosolized by an atomizer (9302, TSI inc., USA) in 2 LPM of compressed clean air. Aerosolized virus particles entered the test duct through a diffusion dryer in order to remove

any moisture, and 3 LPM of clean air was used as sheath air (Fig. 1c). The fabricated air filter sample with or without dust loading was installed in the test duct. Two probes were placed downstream and upstream of the filter sample in order to measure the number concentrations of virus particles by the SMPS system. The filtration efficiency of the filter for virus aerosols was calculated as

$$\eta_{\text{filt}} = 1 - \frac{N_{\text{down}}}{N_{\text{up}}} \tag{11}$$

where N is the number concentration of virus particles (particles/cm^3), and subscripts up and down represent upstream and downstream of the filter sample, respectively.

2.6. Inactivation test

The aerosolized virus particles were deposited onto an air filter sample for 15 mins at standard atmospheric conditions and a relative humidity of approximately 36%. Then, the elution process for virus particles from the filter sample was performed with reference to the work of Kettleson et al. [11]: Urea-arginine phosphate buffer (U-APB) solution was prepared by adding 0.9 g of urea, 0.4 mL of 0.2 M NaH_2PO_4, and 0.5 M L-arginine into 10 mL of DI water. The filter sample was placed into the solution for 10 min. Then 0.1 mL of the solution was dissolved in 0.9 mL of DI water, and the number of plaques in the solution was counted with a single agar layer method [33]: Tryptic soy agar (TSA) solution was inoculated with *Escherichia coli* strain C3000 (ATTCC 15597), and the solution was used as a host bacterial solution after overnight shaking incubation at 37 °C. The next morning, 0.1 mL of U-APB solution containing eluted virus particles was mixed with 0.3 mL of host bacterial solution and 29 mL of TSA containing 8 g/L of agar. The mixture was poured into the petri-dish and incubated overnight at 37 °C. Then, the number of plaques was counted. The percentage of virus particles recovered from the filter sample using U-APB solution was approximately 29%. The anti-viral action by released materials (silver nanoparticles and/or silver ions) during the elution process was negligible (See Supplementary material).

The anti-viral efficiency after a 15 min exposure to virus particles ($\eta_{\text{antiviral,15}}$) was calculated as

$$\eta_{\text{antiviral,15}} = 1 - \frac{\text{PFU}_{\text{sample}}}{\text{PFU}_{\text{pristine}}} \tag{12}$$

where *PFU* is the concentration of virus particles (PFU/m^3), and the subscripts sample and pristine represent the fabricated filter sample and pristine (silver nanoparticle uncoated) filter sample, respectively.

3. Results and discussion

3.1. Fabrication of silver nanoparticle coated air filter

The size distribution of silver nanoparticles generated by the SDG system is shown in Fig. 2 (see upstream). The mode diameter and geometric standard derivation were approximately 11 nm and 1.5, respectively. The number and mass concentrations upstream of the filter sample were 3.34×10^6 particles/cm^3 and 103.6 μg/m^3, respectively, while these concentrations downstream of the filter sample were 3.46×10^5 particles/cm^3 and 60.44 μg/m^3. Therefore, the coating efficiencies of the filter sample for silver particles were approximately 89.6% in number base and 41.7% in mass base. Three filter samples with different coating areal densities of 9.34×10^8, 2.80×10^9, and 4.67×10^9 particles/cm^2 were fabricated in addition to the pristine filter with an areal density of 0.

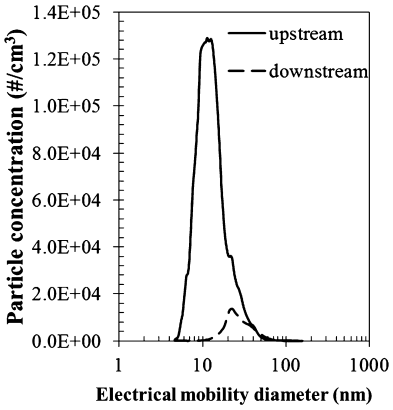

Fig. 2. Silver nanoparticle concentrations upstream and downstream of the filter.

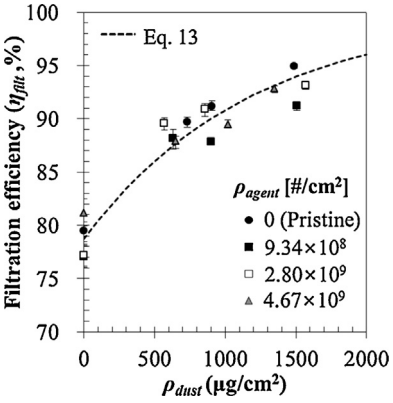

Fig. 3. Filtration efficiency of the filter with dust loading.

3.2. Filtration efficiency and pressure drop

The bacteriophage MS2 virus particles were aerosolized to evaluate filtration efficiency of the filter sample with varying coating areal density and dust loading. The media velocity for the case of no dust loading was set at 0.05 m/s, which is the typical media velocity for the woven-type filters used in heating, ventilating, and air conditioning (HVAC) systems. The mode diameter, geometric standard deviation, and number concentration of aerosolized MS2 virus were approximately 23 nm, 1.58, and 5.23×10^5 particles/cm^3, respectively. Filtration efficiencies of fabricated air filter samples are shown in Fig. 3. The filtration efficiency increased with increasing dust amount (ρ_{dust}), while the efficiency was not much affected by the number of silver nanoparticles coated on the filter sample (ρ_{agent}). In previous research, the filtration efficiency of a dust loaded filter was described as follows [34]:

$$\eta_{\text{filt}} = 1 - P_0 \exp\left[-\beta \rho_{\text{dust}}\right] \tag{13}$$

where P_0 is the penetration for the special case of no dust loading (unused filter), and β is a constant representing filter performance and depends on the filter material. The experimental results were in good agreement with the theoretical prediction when β was set at 8.0×10^{-4} cm^2/μg. Fig. 4 shows that the pressure drop increased with increasing dust load. As with filtration efficiency, the number of coated silver nanoparticles did not have any significant effect on the pressure drop. In this study, the increase in solidity induced by silver nanoparticles coated on a filter sample was on the order of 10^{-7}, while the increase in solidity caused by dust loading was on the order of 10^{-2}, which was slightly higher than that of the pristine filter ($\alpha' \cong 0.0095$). Thus, dust loading can disturb the flow inside

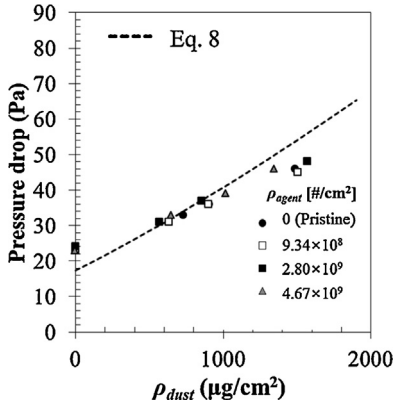

Fig. 4. Pressure drop of the filter with dust loading.

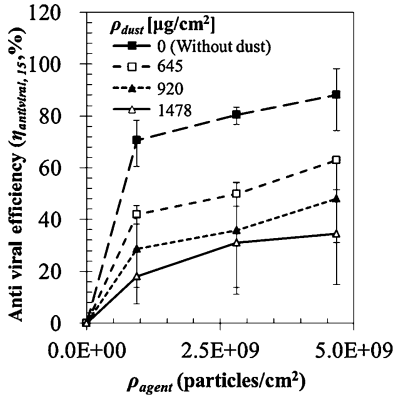

Fig. 5. Anti-viral efficiency after a 15 min exposure ($\eta_{anti,15}$) at various coating areal densities.

the filter media, resulting in increases in filtration efficiency and pressure drop of the filter.

3.3. Anti-viral ability

Anti-viral efficiencies after 15 mins of exposure ($\eta_{antiviral,15}$) with various coating areal densities (ρ_{agent}) and dust amounts (ρ_{dust}) are shown in Fig. 5. As expected, the efficiency increased with ρ_{agent} but decreased with ρ_{dust}. These trends were the same as those reported in our previous study, where the anti-bacterial ability of silver nanoparticles coating an air filter with dust loading was evaluated [17]. In that study, two kinds of bacteria, *E. coli* (*E. coli*, Gram-), *Staphylococcus epidermidis* (*S. epidermidis*, Gram+) were tested. One possible effect of deposited dust particles on the anti-viral ability is that the dust particles can prevent direct contact between silver nanoparticles and virus particles, resulting in the decrease of the anti-viral ability.

Fig. 6 was re-plotted from Fig. 5 using the definition of $\phi_{surv,\tau} = 1 - \eta_{antiviral,15}$. In Fig. 6a, Eq. (5) was used to fit the experimental data points using κ as the fitting parameter. In order to obtain the values of κ at each dust loading condition, τ was set at 15 mins (virus deposition time), and the values of $\dot{N}''_{depo}$ were determined from the experimental results according to the relationship:, where l is the volume of U-APBS containing virus particles eluted from the filter sample (10 mL in this study). The fittings were in good agreement with the experimental data points, when the values of κ were 2.3×10^{-5}, 6.5×10^{-6}, 2.5×10^{-6}, and 1.3×10^{-6}, respectively, for $\rho_{dust} = 0$, 642, 920, and 1478 (μg/cm²). These values of κ and ρ_{dust} are plotted in Fig. 6b. Then, a curve fit was performed with Eq. (6), resulting from the selection of $\gamma = 5.49 \times 10^{-3}$ cm²/μg.

3.4. Filter quality factor

There are two parameters that determine filter performance: pressure drop across the filter and particle filtration efficiency. The best filter is the one that demonstrates the highest filtration efficiency with the smallest pressure drop. However, increasing filtration efficiency inevitably results in increased pressure drop. Thus, the quality factor, which is the ratio of particle penetration to pressure drop, is widely used to compare the performances of various air filters. In this study, two different filter quality factors, filtration quality factor (q_{filt}) and anti-viral quality factor ($q_{antiviral,15}$), were calculated using the following equations:

$$q_{filt} = \frac{\ln\left(1/(1-\eta_{filt}\right)}{\Delta P} \quad (14)$$

$$q_{antiviral,15} = \frac{\ln\left(1/(1-\eta_{antiviral,15}\right)}{\Delta P} \quad (15)$$

Using the results of Figs. 3, 4, and 6a, these two quality factors were calculated, and the results are shown in Fig. 7. The filtration quality factor(q_{filt}) decreased with increasing dust load (Fig. 7a) but was not affected by the amount of silver nanoparticles coated onto the filter (ρ_{agent}). Similarly, the anti-viral quality factor ($q_{antiviral,15}$) decreased with increasing dust load (Fig. 7b) but increased with increasing ρ_{agent}.

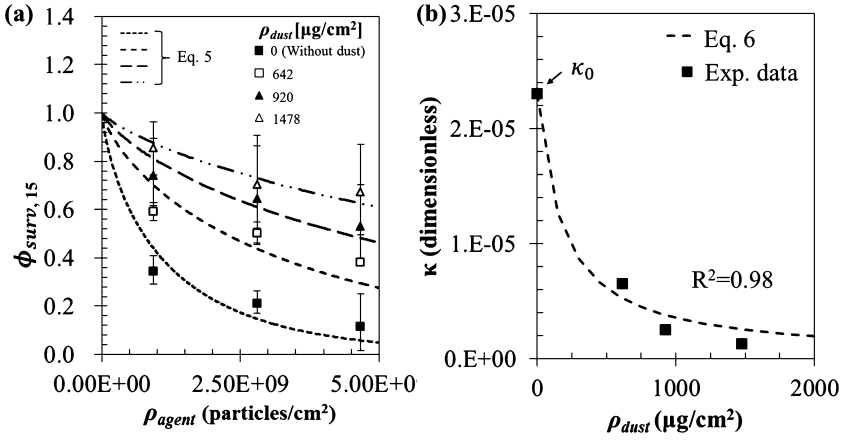

Fig. 6. (a) Survival fraction of virus, and (b) unknown value κ with dust loading.

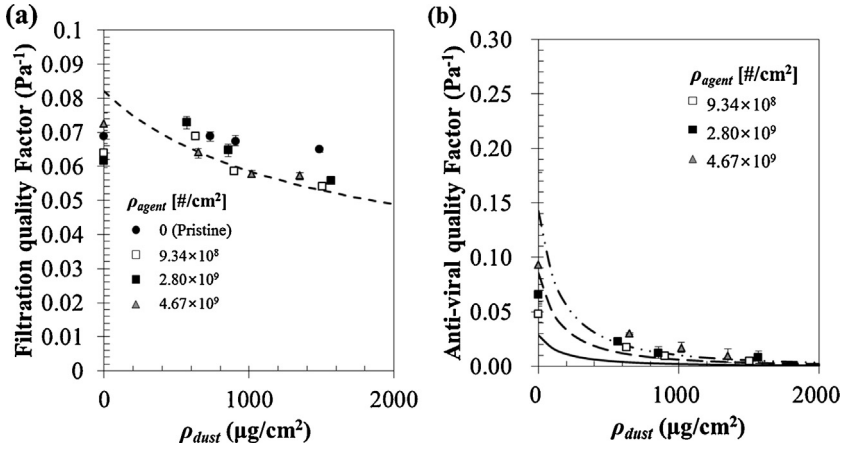

Fig. 7. Quality factors of the filter with dust loading @ V_{media} = 0.05 m/s (a) as a function of filtration efficiency, (b) as a function of anti-viral efficiency.

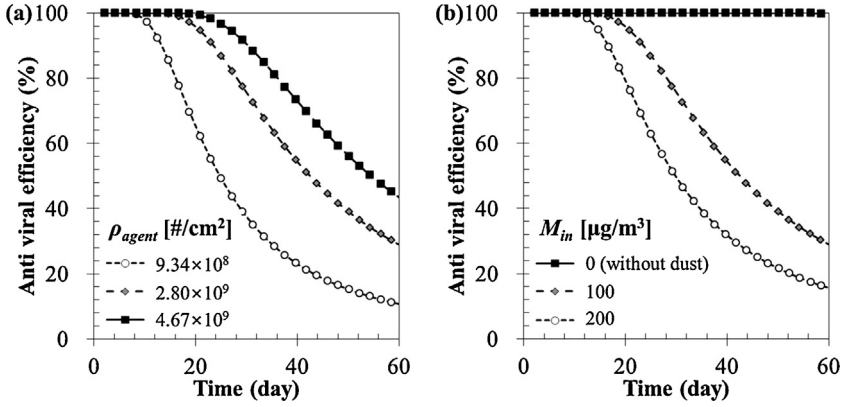

Fig. 8. Calculation results of anti-viral efficiency (a) with various ρ_{agent} when N_{in} = 500 PFU/m^3, M_{in} = 100 μg/m^3, V_{media} = 0.05 m/s, A_{media} = *10* m^2, $\eta_{filt}(t=0)$ = 80% (b) with various M_{in} when N_{in} = 500 PFU/m^3, $\rho_{agent} = 2.8 \times 10^9$, V_{media} = 0.05 m/s, A_{media} = *10* m^2, $\eta_{filt}(t=0)$ = 80%.

3.5. Application of the model

So far, the effects of amounts of anti-viral agent (Ag NPs) and dust particles (Arizona road dust) on filter performance (filtration and anti-viral efficiencies and filter quality factors) have been presented. For this, filtration and anti-viral tests were carried out after preparing filter samples with different amounts of silver nanoparticles and dust loading. However, in a real situation, the areal density of loaded dust (ρ_{dust}) increases with filter operation time (t). When dust particles are deposited on the filter, the areal density of loaded dust can be calculated as

$$\rho_{dust}(t) = \dot{M}''_{depo} \times t \tag{16}$$

where $\dot{M}''_{depo}$(μg/cm^2 min) is the mass flux of dust particles deposited on the filter. Consequently, the anti-viral efficiency of an anti-viral air filter with dust loading can be expressed as follows:

$$\eta_{antiviral}(t) = 1 - \exp\left[-\left(\frac{\kappa_0}{1+\gamma \dot{M}''_{depo} t}\right)\frac{\rho_{areal}}{\dot{N}''_{depo} t}\right] \tag{17}$$

Since $\dot{M}''_{depo}$ is determined using the filtration efficiency, η_{filt}, $\dot{M}''_{depo}$ can be expressed as

$$\dot{M}''_{depo} = \eta_{filt}\dot{M}''_{in} \tag{18}$$

where $\dot{M}''_{in}$ (μg/cm^2 · min) is the mass flux of dust particles approaching the filter.Eq. (17) was used to calculate the anti-viral efficiencies. The total media area of the filter and initial filtration efficiency were chosen to be 10 m^2 and 80%, respectively, and the calculations were performed at a constant inlet virus concentration (N_{in}), 500 PFU/m^3; three inlet dust concentrations (M_{in}) of 0, 100, and 200 μg/m^3; and three coating areal densities (ρ_{agent}) of 9.34×10^8, 2.8×10^9, and 4.7×10^9 particles/cm^2. The calculations reflected the experimental tendencies that the anti-viral ability of the filter increased with coating areal density (Fig. 8a) and decreased with dust loading (Fig. 8b).

Our model can be applied to determine two major issues in filter operation: (1) The anti-viral abilities of various anti-viral filters can be quantitatively compared by comparing κ values (higher means κ higher anti-viral ability). (2) The replacement cycle of an anti-viral air filter can be determined by considering the effects of dust loading on pressure drop and anti-viral ability.

Acknowledgements

This research was supported by Future-based Technology Development Program (Green Nano Technology Development Program) through the National Research Foundation of Korea (NRF) funded by the Ministry of Education, Science and Technology (grant number 2010-0029297), and Korea Ministry of Environment (MOE) as Advanced Technology Program for Environmental Industry.

Appendix A. Supplementary data

Supplementary data associated with this article can be found, in the online version, at http://dx.doi.org/10.1016/j.jhazmat.2015.09.017.

References

[1] W.W.-F. Leung, C.-H. Hung, P.-T. Yuen, Experimental investigation on continuous filtration of sub-micron aerosol by filter composed of dual-layers including a nanofiber layer, Aerosol Sci. Technol. 43 (2009) 1174–1183.
[2] N. Lee, D. Hui, A. Wu, P. Chan, P. Cameron, G.M. Joynt, A. Ahuja, M.Y. Yung, C. Leung, K. To, A major outbreak of severe acute respiratory syndrome in Hong Kong, New Engl. J. Med. 348 (2003) 1986–1994.
[3] G.J. Smith, D. Vijaykrishna, J. Bahl, S.J. Lycett, M. Worobey, O.G. Pybus, S.K. Ma, C.L. Cheung, J. Raghwani, S. Bhatt, Origins and evolutionary enomics of the 2009 swine-origin H1N1 influenza A epidemic, Nature 459 (2009) 1122–1125.
[4] H.J. Chao, J. Schwartz, D.K. Milton, H.A. Burge, Populations and determinants of airborne fungi in large office buildings, Environ. Health Perspect. 110 (2002) 777–782.
[5] C.E. Main, Aerobiological, ecological, and health linkages, Environ. Int. 29 (2003) 347–349.
[6] J. Douwes, P. Thome, N. Pearc, D. Heederik, Review: bioaerosol health effects and exposure assessment: Progress and prospects, Ann. Occup. Hyg. 47 (2003) 187–200.
[7] F. Fung, W.G. Hughson, Health effects of indoor fungal bioaerosol exposure, Appl. Occup. Environ. Hyg. 18 (2003) 535–544.
[8] T. Husman, Health effects of indoor-air microorganisms, Scand. J. Work Environ. Health 22 (1996) 5–13.
[9] W.F. Wells, Airborne Contagion and Air Hygiene, Cambridge University Press, Cambridge, 1955.
[10] G. Oberdörster, M.J. Utell, Ultrafine particles in the urban air: to the respiratory tract and beyond? Environ. Health Persp. 110 (2002) A440.
[11] E.M. Kettleson, B. Ramaswami, C.J.J.R. Hogan, M.H. Lee, G.A. Statyukha, P. Biswas, L.T. Angenent, Airborne virus capture and inactivation by an electrostatic particle collector, Environ. Sci. Technol. 43 (2009) 5940–5946.
[12] S.A. Grinshpun, A. Adhikari, C. Li, M. Yermakov, L. Reponen, E. Johansson, M. Trunov, Inactivation of aerosolized viruses in continuous air flow with axial heating, Aerosol Sci. Technol. 44 (2010) 1042–1048.
[13] O.V. Pyankov, E.V. Usachev, O. Pyankova, E. Agranovski, Inactivation of airborne influenza virus by tea tree and eucalyptus oil, Aerosol Sci. Technol. 46 (2012) 1295–1302.
[14] K.T. Park, J. Hwang, Filtration and inactivation of aerosolized bacteriophage MS2 by a CNT air filter fabricated using electro-aerodynamic deposition, Carbon 75 (2014) 401–410.
[15] Y.H. Joe, K. Woo, J. Hwang, Fabrication of an anti-viral air filter with SiO2-Ag nanoparticles and performance evaluation in a continuous airflow condition, J. Hazard. Mater. 280 (2014) 356–363.
[16] K.K. Foarde, J.T. Hanley, Determine the efficacy of antimicrobial treatments of fibrous air filters, ASHRAE Trans. 107 (2001) 156–170.
[17] W. Joe, J.H. Ju, Y.H. Park, Correlation between the antibacterial ability of silver nanoparticle coated air filters and the dust loading, Aerosol Air Qual. Res. 13 (2013) 1009–1018.
[18] L. Lu, R.W. Sun, R. Chen, C.K. Hui, C.M. Ho, J.M. Luk, G.K. Lau, C.M. Che, Sil-ver nanoparticles inhibit hepatitis B virus replication, Antivir. Ther. 13 (2008) 253–262.
[19] C. Baker, A. Pradhan, L. Pakstis, D.J. Pochan, S.I. Shah, Synthesis and antibac-terial properties of silver nanoparticles, J. Nanosci. Nanotechnol. 5 (2005) 244–249.
[20] M. Rai, A. Yadav, A. Gade, Silver nanoparticles as a new generation of antimi-crobials, Biotechnol. Adv. 27 (2009) 76–83.
[21] C. Aymonier, U. Schlotterbeck, L. Antonietti, P. Zacharias, R. Thomann, J.C. Tiller, S. Mecking, Hybrids of silver nanoparticles with amphiphilic hyperbranchedmacromolecules exhibiting antimicrobial properties, Chem. Commun. (Camb.) (2002) 3018–3019.
[22] J.P. Ruparelia, A.K. Chatterjee, S.P. Duttagupta, S. Mukherji, Strain specificityin antimicrobial activity of silver and copper nanoparticles, Acta Biomater. 4 (2008) 707–716.
[23] G. Borkow, J. Gabbay, Putting copper into action: copper-impregnated productswith potent biocidal activities, FASEB J. 18 (2004) 1728–1730.
[24] H. Horvath, M. Gangl, A low-voltage spark generator for production of carbon particles, J. Aerosol Sci. 34 (2003) 1581–1588.
[25] J.-T. Kim, J.-S. Chang, Generation of metal oxide aerosol particles by a pulsed spark discharge technique, J. Eletrostat. 63 (2005) 911–916.
[26] J.-P. Borra, Nucleation and aerosol processing in atmospheric pressure electrical discharges: Powders production, coatings and filtration, J. Phys. D-Appl. Phys. 39 (2006) R19–R54.
[27] L. Simonin, U. Lafont, U. Tabrizi, A. Schmidt-Ott, E.M. Kelder, Sb/O nano-composites produced via spark discharge generation for Li-ion battery anodes, J. Power Sources 174 (2007) 805–809.
[28] J.H. Byeon, J.H. Park, J. Hwang, Spark generation of monometallic and bimetallic aerosol nanoparticle, J. Aerosol. Sci. 39 (2008) 888–896.
[29] N.S. Tabrizi, M. Ullmann, V.A. Vons, U. Lafont, A. Schmidt-Ott, Generation of nanoparticles by spark discharge, J. Nanopart. Res. 11 (2009) 315–332.
[30] S. Sharif, Chemical and mineral composition of dust and its effect on the dielectric constant, IEEE Trans. Geosci. Remote Sensing 33 (1995) 353–359.
[31] B.A. Begum, S.K. Biswas, P.K. Hopke, D.D. Cohen, Multi-element Analysis and Characterization of Atmospheric Particulate Pollution in Dhaka, Aerosol Air Qual. Res. 6 (2006) 334–359.
[32] R.C. Brown, Air Filtration: An Integrated Approach to the Theory and Applications of Fibrous Filters, Pergamon Press, New York, 1993.
[33] U.S. EPA, Manual of Methods for Virology, Chapter 16. procedures for detecting coliphages, EPA 600/4-84/013, U.S. Environmental Protection Agency, Washington, DC, 2001.
[34] R.C. Brown, W.R. Gray, D.B. Blackford, G.J. Bostock, Effect of industrial aerosols on the performance of electrically charged filter material, Ann. Occup. Hyg. 32 (1988) 271–294.